Biosensors and Bioelectronics 79 (2016) 661–668

Contents lists available at ScienceDirect

Biosensors and Bioelectronics

journal homepage: www.elsevier.com/locate/bios

Single functional magnetic-bead as universal biosensing platform for trace analyte detection using SERS-nanobioprobe

R. Xiao [a,1], C.W. Wang [a,1], A.N. Zhu [b], F. Long [b,*]

[a] Beijing Institute of Radiation Medicine, Beijing 100850, China
[b] School of Environment and Natural Resources, Renmin University of China, Beijing 100872, China

ARTICLE INFO

Article history:
Received 5 November 2015
Received in revised form
30 December 2015
Accepted 31 December 2015
Available online 31 December 2015

Keywords:
Surface-enhanced Raman scattering
Nanobiosensor
Magnetic-bead
Small molecule
Protein

ABSTRACT

SERS biosensor has demonstrated remarkable potential to analyze various bio/chemical targets with ultrahigh sensitivity. However, the development of universal SERS biosensing platforms with a uniform and reproducible structure that can quantitatively detect a broad range of trace analytes remains a significant challenge. The production of SERS nanotags with abundant Raman reporters and rational structure to conjugate with detection biomolecules is another key to design SERS-nanobioprobes. Here, we introduce a facile single magnetic-bead biosensing platform, formed by combining the captured antibodies/antigens conjugated magnetic-beads and the Au@Raman-Reporters@Ag sandwich-based nanorod tags labeled nanobioprobes. The advantage of the robust sandwich-structure-based nanotags is attributed not only to the high density Raman reporters contained inside, with high EF value because of enhanced electromagnetic field density, but also to the flexibility for bioconjugation of the detection biomolecules. The 3-D structure of the functional magnetic-bead provides a perfect platform to rapidly capture and enrich biomolecules. Ultrasensitive detection of two small molecules and a protein was achieved in samples, respectively.

1. Introduction

Ultrasensitive detection of trace analytes is essential in many fields, from clinical diagnostics and drug discovery, to public safety and environmental protection (Overington et al., 2006; Swierczewska et al., 2012; Longo et al., 2013; Ndieyira et al., 2014). Surface-enhanced Raman scattering (SERS) has demonstrated tremendous potential for the analysis of various biological and chemical targets, including small molecules, DNA, proteins, and cells, at the trace, and even at single-molecule levels (Nie and Emery, 1997; Qian and Nie, 2008; Grubisha et al., 2003; Zhang et al., 2013). SERS-based nanobiosensors originate from the combination of SERS, nanomaterial and biomaterial forms. Generally, the SERS-based biosensor may be grouped into three fundamental classes: planar SERS-active surfaces acting as biosensing platforms, SERS nanotags serving as labels on biomolecules, and the combination of both. Biosensors based on planar SERS-active surfaces have been widely developed (Grubisha et al., 2003; Anker et al., 2008; Stewart et al., 2008; Li et al., 2013). Because nanostructural geometry can markedly affect Raman signals, a lack of control over factors such as size and shape variation of nanostructures, non-identical internanostructural distances, and inhomogeneous distributions of analyte molecules on surfaces can adversely influence optimal performance of these structures (Anker et al., 2008; Stewart et al., 2008; Li et al., 2013). These biosensors with both high sensitivity and high reproducibility typically require sophisticated and expensive nanofabrication techniques. Furthermore, given the 2-D configurations, the available density of SERS-active sites within the detection volume is limited (Li et al., 2013). Additionally, the 2-D SERS substrates rely on the analytes' ability to diffuse slowly to in bulk solution to reach the SERS-active sites. Therefore, the corresponding SERS detection method is time-consuming and unfavorable for fast, in-line, real-time analysis. Construction of a universal SERS biosensing platform with a uniform and reproducible structure that can quantitatively detect a broad range of trace analytes is still considered a costly and significant challenge.

SERS nanotag, integration of silver or gold nanostructures and Raman active molecules, has been recently explored for detection, sensing, and imaging (Stewart et al., 2008; Li et al., 2013; Marc et al., 2013; Wang et al., 2013). The SERS nanotage system possesses several intrinsic benefits in quantitative assay of trace analytes. First, "hot spots" generated in the nanoscale junctions and interstices of the SERS nanostructures afford enormous Raman enhancement factors on the order of 10^{14}–10^{15}, leading to superb

* Corresponding author. Fax: +86 10 62771472.
E-mail address: longf04@mails.thu.edu.cn (F. Long).
[1] These authors contributed equally to this work.

http://dx.doi.org/10.1016/j.bios.2015.12.108
0956-5663/

detection sensitivity (Nie and Emery, 1997; Qian and Nie, 2008; Zhang et al., 2013). Second, the robust structures of SERS nanotags and their high densities of the SERS active molecules provide unique and uniform signals, which are significant valuable in quantitative analysis (Li et al., 2013). Third, when conjugated with biomolecular targeting ligands such as monoclonal antibodies, peptides, DNA sequences or small molecules, these SERS nanotag labeled nanobioprobes can be used to target their receptors with high specificity and affinity (Anker et al., 2008). Additionally, given the highly resolved Raman spectral signature and the wide excitation wavelength of SERS active molecules, SERS nanobioprobes are ideally suited for simultaneous detection of multiple species in complex samples (Marc et al., 2013; Li et al., 2012). Au@Ag core-shell nanotags have elicited considerable attention for their higher SERS activity than that of monometallic gold nanoparticles (Marc et al., 2013). In terms of plasmonic nanoparticle geometries, the Au@Ag NRs is considered to be most suitable because of its controllable monodispersity and aspectratio, broad plasmon resonance tenability from near-UV to the IR range, and increased sharpness and strength of longitudinal SPR bands (Wu et al., 2012). Some immunoassay methods have been reported using Au@Ag NRs nanobioprobes (Grubisha et al., 2003; Wu et al., 2012; Li et al., 2012). However, most of those assays labeled the SERS report molecules on the surface of Au@Ag NRs and did not match their LSPR with the Raman excitation wavelength (Qian and Nie, 2008). Moreover, the aggregation of nanobioprobes will form nanojunctions between two plasmonic surfaces to generate additional SERS "hotspots" (Li et al., 2010), which thus lead to an abnormally high level of SERS signals and inevitably affects the accuracy of detection results.

An ideal SERS-based biosensing platform would consist of a reproducible and standardized substrate with controllable and highly active SERS-based nanobioprobes. Herein, a facile and reproducible single magnetic-bead biosensing platform (SMBP) has been developed for ultrasensitive and highly selective bioassay of trace analytes. Single uniformly sized magnetic-beads with captured antibodies/antigens served as nanobiosensing substrate. The sandwich structure of Au@Raman reporters@Ag core-shell nanorods (Au@RR@Ag NRs) was assembled layer-by-layer relative to the Raman tags. The combination of functional magnetic-beads and Au@RR@Ag NRs based bionanoprobes has allowed the highly sensitive and selective detection of trace analytes, including small molecules and proteins. The 3-D structure of the functional magnetic-beads provides a perfect platform for the capture and enrichment of biomolecules and allows rapid binding between antibody and antigen in homogeneous solution by reducing the space steric effect. The sandwich structure of Au@RR@Ag NRs facilitates modification of various biomolecules through well-known self-assembling chemistry and preparation of the needed SERS-based nanobioprobes. This sandwich structure can embed a number of active Raman reporters with high EF value related to enhanced electromagnetic field density, thereby improving the sensitivity of the SERS nanobiosensor, while greatly inhibiting the unwanted Raman signals induced by "hot spots" formed from the aggregation of nanobioprobes. We demonstrated the ability of the SMBP in ultrasensitive detection of small molecules and proteins with established mechanisms.

2. Experimental sections

2.1. Materials and chemicals

N-hydroxysulfosuccinimide sodium salt (sulfo-NHS), N-(3-dimethylamino propyl)-N'-ethylcarbodiimide hydrochloride (EDC), Tween® 20, Bovine serum albumin (BSA), 1-ethyl-3 (-3dimethylamino-propyl) carbodiimide hydrochloride (EDC), ovalbumin (OVA), p-Aminothiophenol (PATP) or 5,5′-dithiobis (2-nitrobenzoic acid) (DTNB), 3-Mercaptopropionic acid (MPA), CTAB, $HAuCl_4$, $NaBH_4$, and $AgNO_3$ was purchased from Sigma (Shanghai, China). MC-LR, MC-RR, MC-YR, MC-LW, MC-LF, and nodularin were obtained from Alexis (ALX-350-012). Dialysis Kit with 5 kDa molecular weight cut-off was purchased from GE Healthcare (USA). All solutions were prepared with ultrapure water from a Millipore Milli-Q sytem. All the other reagents, unless specified, were supplied by the Beijing Chemical Agents (China). All chemicals were of analytical reagent (AR) grade.

Monoclonal anti-MC-LR antibody and monoclonal anti-BPA antibody were produced by our research group. Mouse immunoglobulin G and goat anti-mouse immunoglobulin G was purchased from Sigma (Shanghai, China). All protein samples were used as received without further purification and diluted in the assay buffer (1 μM phosphate buffer solution with pH 7.4) prior to sensing measurement. Human serum (from clotted human male whole blood, 40–90 mg/ml total protein) was also purchased from Sigma (Shanghai, China).

2.2. Synthesis of sandwich-structure based Au@RR@Ag NRs nanotags

Gold nanorods (Fig. S1) were synthesized by a previously reported seeding growth method (Babak and Mostafa, 2003). To prepare Au@RR@Ag sandwich structure, 20 mL of the as-prepared Au NRs were centrifuged twice at 8000 rpm for 10 min to remove the excess reagents. The precipitate was re-dispersed in 10 mL of deionized water. Subsequently, 10 μL of 10 mM p-Aminothiophenol (PATP) or 5,5′-dithiobis (2-nitrobenzoic acid) (DTNB) ethanol solution was added and the mixture was reacted for 2 h under continuous stirring. The PATP (or DNTB) modified Au NRs were rinsed by centrifugation and re-suspension with the same volume of deionized water. Au@RR@Ag NRs were then prepared as previously described (Xiang et al., 2008) with some modifications. Briefly, 2 mL of the PATP (or DNTB) modified Au nanorods solution was added to 4 mL of 0.04 M CTAB aqueous solution with vigorous stirring at 28 °C. Up to 130 μL of 0.1 M ascorbic acid, varying amounts of 1 mM $AgNO_3$, and 240 μL of 0.1 M NaOH were added sequentially. The color of the solution gradually changed in 2 min, indicating the formation of Au@RR@Ag NRs. Followed by purification, the core-shell nanorods solution was concentrated to 2 mL with deionized water. Au@RR@Ag NR nanotags was carboxyled by MPA for next modification.

2.3. Conjugation of SERS nanotags with detection antibodies (denoted as SERS nanobioprobes)

The SERS nanobioprobes were prepared by conjugating an amine of antibodies to carboxyl-coated Au@RR@Ag NR nanotags through the EDC/sulfo-NHS chemistry. The EDC and Sulfo-NHS reagents were used together, to enhance the conjugation efficiency. 50 μL of 8 μM stock solution of Au@RR@Ag NR nanotags were diluted to 0.5 mL using a 10 mM borate buffer (pH 7.4), and up to 0.5 mL of 3 mg/mL antibodies was added. After being well-mixed, 10 μL of a 10 mg/mL as-prepared EDC/NHS solution was added to the mixture, which was gently stirred for 1.5 h at room temperature for conjugation. To block the unreacted carboxyl sites on the Au@RR@Ag NR nanotags surface, 0.5 mL of 10 mg/mL BSA was added to the mixture and allowed to react for an additional 1 h. The mixture then was filtered through a 0.2 μm PES syringe filter to remove any large aggregates before being transfer to a clean centrifugal ultrafiltration unit (100 kDa cutoff; GE Healthcare, USA). To remove any excess unbound antibody, the solution was centrifuged at 3000 rpm for five buffer exchanges (50 mM borate buffer, pH 8.3). After completing ultracentrifugation, the

solution was filtered through a 0.2 μm syringe filter to remove any aggregates. The products were stored at 4 °C before use.

2.4. Magnetic-beads modified by captured biomolecules

Standard protocols were used to covalently attach the amine groups on the magnetic bead surface to capture antibody (for protein detection) or coated-antigen (for small-molecule

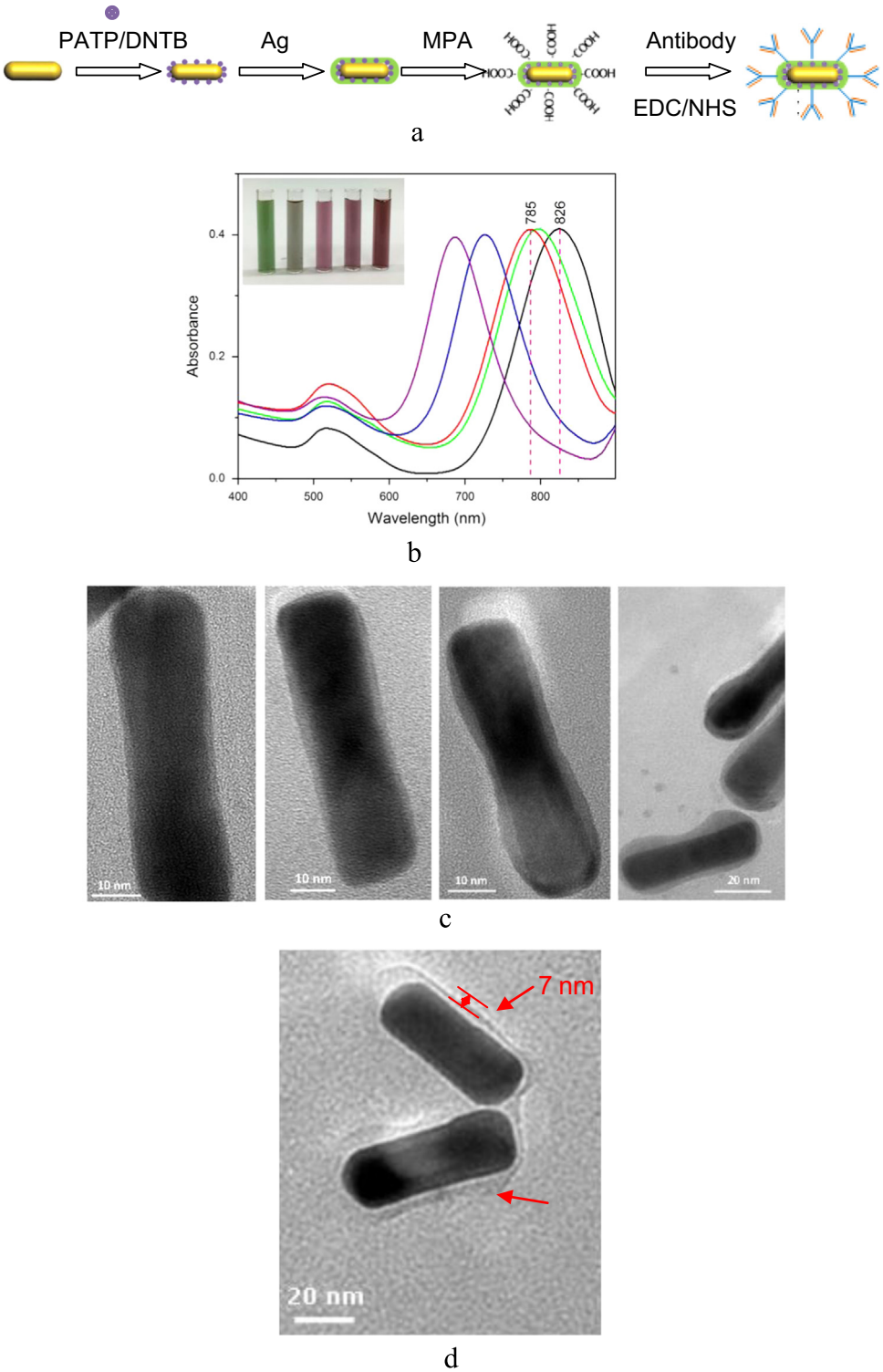

Fig. 1. Preparation and characterization of Au@RR@Ag NRs based nanobioprobes. a, Synthesized schematic of Au@RR@Ag NRs based nanobioprobes. Au@Ag Core–shell nanoparticles were prepared by coating Au nanorods with Ag after PATP (or DNTB) molecules anchored to Au surface via S-Au covalent bonding. Then, detection antibodies were conjugated with carboxyled Au@RR@Ag NRs nanotags. b, Extinction spectra of gold nanorods (black curve) and Au@RR@Ag NRs with different thickness (1.1, 1.9, 3.1, and 6.3 nm) of Ag shell (other curves). In the inset of Fig. 1b, gold nanorods (right), and Au@RR@Ag NRs with plasmon resonance located at 797, 785, 750, and 662 nm, respectively, show true color changes with changing silver shell thickness. c, TEM photos of Au@RR@Ag NRs, the thickness of silver layer is from 1.9 nm to 6.3 nm. d, TEM photos of Au@RR@Ag NRs based nanobioprobes modified by antibodies, the red arrow points to the antibody layer.

detection). Nonspecific sites on the bead surface were blocked by using BSA (0.5 mg/ml) in PBS buffer (pH 7.4). Excess unbound protein was removed by magnetic separation.

2.5. Characterization

High-resolution transmission electron microscopy (HR-TEM) images were obtained using a JEM-2100F transmission electron microscope at an accelerating voltage of 200 kV. Samples dispersed at an appropriate concentration were cast onto a carbon-coated copper grid. Scanning electron microscopy (SEM) images were captured using an S-4800 scanning electron microscope (Hitachi, Japan). UV–vis spectra were measured on a Shimadzu UV-3150 spectrometer. Raman spectra were recorded using the Invia Reflex by Renishaw with 785 nm laser excitation and a $50\times$ objective. The data acquisition time was usually 10 s and the peak intensities of samples were normalized with respect to that of the silicon wafer at 520 cm^{-1}. The magnetic-beads samples were dispersed uniformly in an Au coated glass plate for SERS measurement.

3. Results and discussion

3.1. Plasmonic nanostructures and their conjugation with detection antibodies as nanobioprobes

A new SERS nanotag (Au@RR@Ag NRs) was synthesized by sandwiching strong Raman reporters (PATP or DNTB) in between Au@Ag core-shell nanorods. Fig. 1a shows the design and preparation of Au@RR@Ag NRs and their schematic structures. The gold nanorods show a longitudinal SPR (LSPR) peak at 826 nm and a transverse one at 516 nm (Fig. S1). The thickness of the silver shell can easily be controlled by varying the volumes of $AgNO_3$ and ascorbic acid, which makes the LSPR of Au@Ag NRs tunable for obtaining maximum SERS signals at a given excited wavelength. However, most of the previous works did not make the LSPRs match the excitation wavelength of the Raman scattering device, and immobilized the Raman reporter molecules on the surface of Au@Ag NRs, which unavoidably prevented the next bioconjugation. The sandwich structure of the Au@RR@Ag NRs is a perfect solution for these defects. We can clearly see that upon increase of the thickness of the sliver shell, a gradual change in the color of colloid solution from brown to green and a change in location of the plasmon resonance of Au@RR@Ag NRs from 826 nm to 662 nm were observed (Fig. 1b). The change in thickness of the silver shell in the nanorods was further demonstrated by TEM photos (Fig. 1c). At sliver shell thickness of 1.9 ± 0.3 nm, the LSPR of Au@RR@Ag NRs located at 785 nm produced the strongest SERS peaks and the EF value of peaks at 1077 cm^{-1} (For PATP) were calculated to be about 2.83×10^6 (Fig. S2–S3). The Raman reporters were embedded into the plasmonic Au@Ag core-shell nanostructures to amplify SERS signal. The silver shell prevented leakage of the Raman reporter molecules and enhanced adsorption of external species, and provided a perfect platform for bioconjugation. Despite the possibility for nanobioprobe aggregation and consequent SERS hot spots formation, any unwanted SERS signal enhancement will be deterred, owing to the Raman reporters' sandwiched location within the Au@Ag core-shell. Additionally, a number of Raman reporter molecules are concentrated in a single sandwich nanoparticle to form the SERS probe. As a result, SERS signal will originate from a collection of Raman reporter molecules, even in a single antibody-antigen binding events, resulting to effective improvement sensitivity. The other advantage of this sandwich structure is the storage stability of SERS-based tags, which is essential for the practical application of Raman-based biosensor. Because the Raman reporters were sandwiched into the Au@Ag structure, the Raman signal strength of the Au@RR@Ag NRs are kept constant despite appearance of any changes on the surface of the silver shell. Our results show that Au@RR@Ag NRs can be stored for a period of three months without any obvious loss of Raman signal (Fig. S4).

To bioconjugate the biomolecules to Au@RR@Ag NRs nanotags, the tags were first carboxyled by 3-mercaptopropionic acid (MPA). Then, the detection antibodies were conjugated to the Au@RR@Ag NRs nanotags by the carbodiimide chemistry, shown in Fig. 1a. The successful conjugation was confirmed by TEM (Fig. 1d). Antibody layer is uniformly distributed around Au@RR@Ag NRs nanotags. The antibody layer is about 6–10 nm, which is consistent with the hydration diameter of the antibody (Murphy et al., 1988). This proves that the captured antibody is conjugated with a single molecule layer form. UV–vis spectra (Fig. S5) demonstrated that the 280 nm adsorption spectra appeared after Au@RR@Ag NRs were modified by the antibodies. The Au@RR@Ag NRs plasmonic resonance spectra remained essentially unchanged after modification of the antibodies except for the slight expansion of half peak width.

3.2. Design of single magnetic-bead biosensing platform (SMBP)

To show the universal applicability of our methods, we chose commercially available magnetic-beads as SERS biosensing substrate. Magnetic-beads have been widely used in the bio-reagent separation and bioassay because of their desirable characteristics, such as reproducibility, cost-effectiveness, uniformity in size, simplicity of use, and ease of use for separation (Matteo et al., 2014). In using single magnetic-beads as SERS biosensing platform, uniformity in size and good dispersity must be considered to ensure comparable results. Both TEM and SEM photos showed that the dispersity of the amine magnetic-beads was sufficient to achieve single magnetic-bead detection (Fig. S6). The magnetic-beads were uniform in size, with diameter of about 2.8 ± 0.2 μm.

To confirm effectiveness and sensitivity of SMBP, we used magnetic-bead-mouse immunoglobulin G (M-IgG) and goat anti-mouse immunoglobulin G (GaM-IgG) SERS nanobioprobes as models for capture and reporting agents. The amine magnetic-bead was modified by the M-IgG with the well-established glutaraldehyde spacer method. GaM-IgG SERS nanobioprobes were prepared according to experimental methods. The mixture of magnetic-bead-M-IgG and various concentrations of GaM-IgG SERs nanoprobes was allowed to react for 30 min, and then separated with a magnet. Next, the magnetic-bead was washed several times by PBS buffer, and the complex was dispersed onto the 50 nm gold layer deposited glass plate (Fig. S7). The gold layer was used to remove the background Raman signal of the glass plate (Fig. S7). The single magnetic-bead Raman signals were detected by Raman spectroscopy. TEM and SEM photos clearly demonstrated that the SERS nanobioprobes bound with captured antibodies immobilized onto the magnetic beads (Fig. 2a,b). An acceptable sample-to-sample variation was obtained by measuring eight separate samples at each concentration (Fig. 2d), revealing relatively good reproducibility of this SERS-based detection strategy. To explore the sensitivity limit of the SERS-based protein detection, Fig. 2c shows Raman signals of SMBP modified by M-IgG after exposure to various concentrations of GaM-IgG SERS nanobioprobes from 1 fg/ml to 5×10^5 fg/ml. At lower concentrations, Raman signals were weak, consistent with a small number of GaM-IgG SERS nanobioprobes captured by the M-IgG layer on the SMBP. Defining the limit of detection as $3\sigma/S$ calculation parameter (average standard deviation of measurements (σ) and slope of the linear range of the dose-response (S) fitting curve), we reproducibly obtained GaM-IgG detection sensitivity of down to

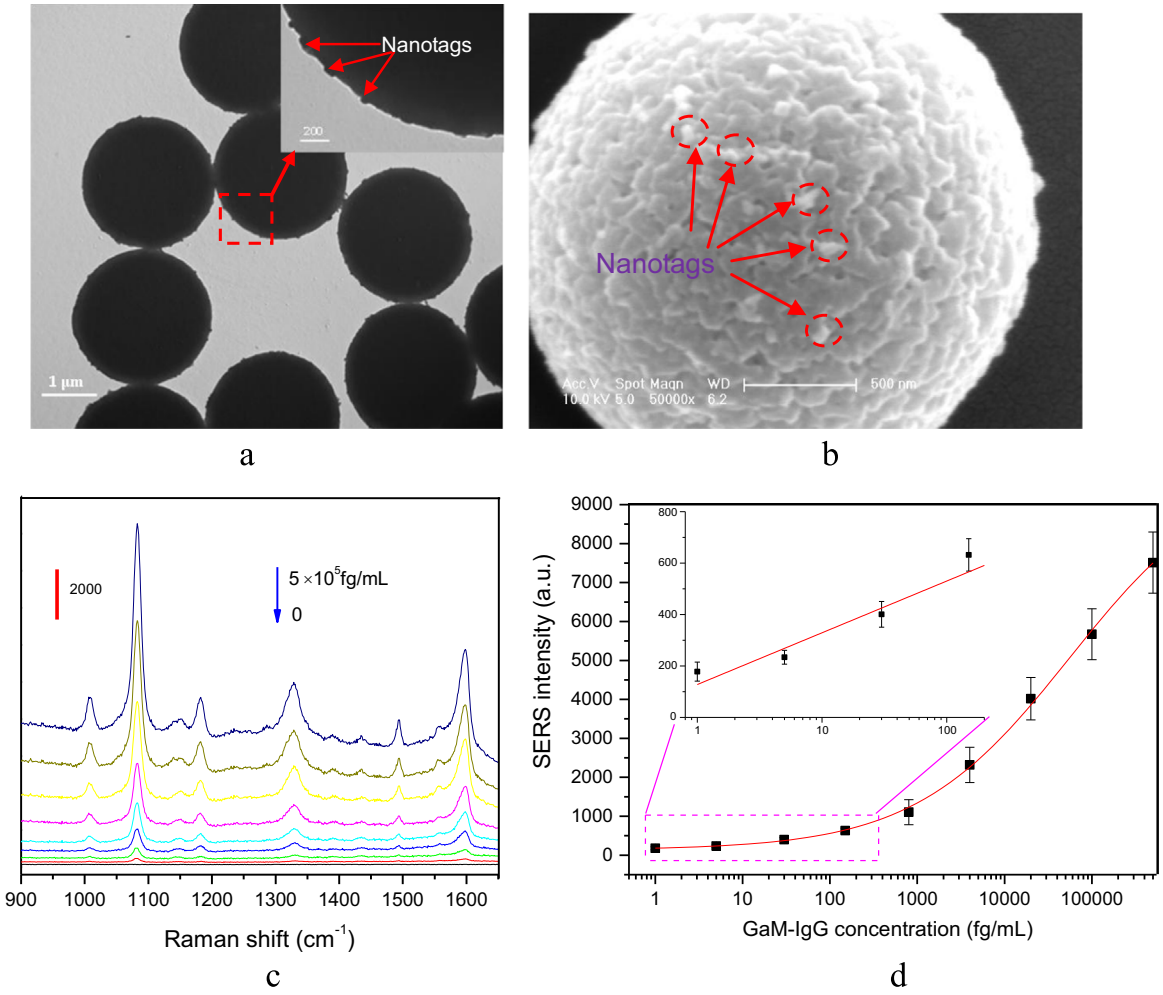

Fig. 2. SMBP for detection of protein antibodies. a and b, TEM and SEM photos of captured magnetic-bead bound to SERS nanobioprobes, respectively. c, Increasing Raman signal with increasing concentrations of GaM-IgG SERS nanobioprobes (1, 5, 30, 1.5×10^2, 8×10^2, 4×10^3, 2×10^4, 1×10^5, and 5×10^5 fg/ml). d, Dose-response curve of SMBP for the concentrations of GaM-IgG SERS nanobioprobes. A sigmoidal dependence was observed and fit by four-parameter logistic function. The error bars represent the standard deviations from 8 measurements.

1 fg/ml, over five orders of dynamic range (Fig. 2d). Notably, Concentrations of nanobioprobe lower than 150 fg/ml produced good linear relations that are already sufficient for quantization of GaM-IgG SERS nanobioprobes (inset of Fig. 2d). The high sensitivity of detection may be attributed to the thousands of Raman reporter molecules encapsulated within each Au@RR@Ag NRs nanotag, and consequently, high signal amplification was achieved when the antibody-conjugated GaM-IgG SERs nanobioprobes bound to M-IgG on the surface of the SMBP. Furthermore, TEM and SEM images (Fig. 2a,b) of the M-IgG-coated magnetic-bead surfaces after incubation with the GaM-IgG SERS nanobioprobes showed that many antibody-conjugated nanobioprobes were bound to a single magnetic bead, providing further significant Raman signal amplification.

3.3. *Small-molecule detection using SMBP*

Ultrasensitive detection of small molecules is essential for environmental monitoring, public safety, and drug development (Overington et al., 2006; Swierczewska et al., 2012; Longo et al., 2013). Therefore, in this study, we showed the feasibility of the SMBP for the detection of small molecules. Microcystin-leucine-arginine (MC-LR; MW=995.2) is one of the most frequently detected and most toxic cyanotoxin in cyanobacterial blooms (Liu et al., 2000; WHO, 2004). To minimize public risk, the World Health Organization (WHO) has set a guideline value (GV) of 1.0 μg/L for MC-LR in drinking water (WHO, 2004). The coated-antigen MC-LR-BSA was prepared according to previous methods (Long et al., 2009). The amine magnetic-beads were conjugated with coated-antigens (MC-LR-BSA) using glutaraldehyde and was used as capture probes. Notably, the concentration of coated-antigen solutions applied in our protocols was exceedingly high to ensure complete coverage of coated-antigen on the substrate surface. Excessive coated-antigens were removed by magnetic separation and washed with the PBS buffer solution.

To achieve the MC-LR quantitative detection, a competitive immunoassay mechanism for MC-LR detection based on SMBP was used, as shown in Fig. 3. During one detection cycle, MC-LR solutions of different concentrations, 1 μg/ml Au@PATP@Ag NR labeled antibody and antigen-coated-magnetic beads were mixed and incubated for a certain time. During incubation, both the free MC-LR in solution and antigens immobilized onto magnetic beads surface bound competitively onto the Au@PATP@Ag NRs nanobioprobes. Once equilibrium state of this competitive antigen-antibody reaction was reached, the magnetic-beads were separated by a magnet and the supernatant was removed. The magnetic-beads were dispersed onto the gold plate after washed several times by PBS buffer. The single magnetic-bead Raman signals were detected by Raman spectroscopy. To reduce the error, eight magnetic-beads were subjected to detection for each concentration of

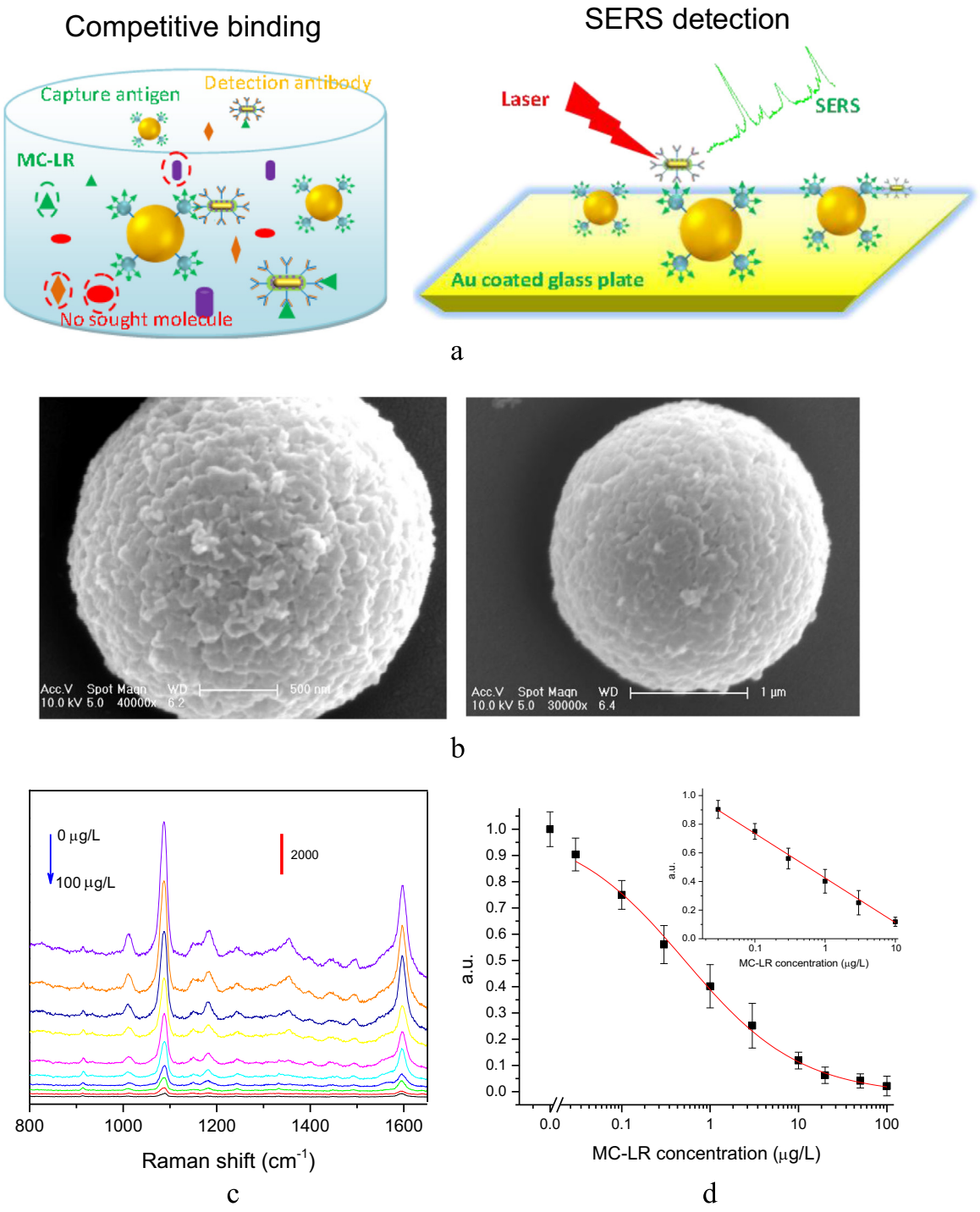

Fig. 3. Schematic representation of the competitive detection of MC-LR using SMBP and SERS signal intensity under the different concentration MC-LR. a, The amine magnetic-beads are functionalized with coated-antigen (MC-LR-BSA). The functional magnetic-beads and SERS nanobioprobes modified by anti-MC-LR antibodies are mixed with the samples containing different concentration MC-LR. Coated-antigen and MC-LR simultaneously compete to bind with SERS nanobioprobes. Then, the complex of magnetic-bead and SERS nanobioprobe was separated by magnet and washed by PBS. Finally, the complex was dispersed on Au-coated glass plate and SERS intensity was detected. b, SEM photos of the complex of magnetic-bead and anti-MC-LR antibody SERS nanobioprobes without MC-LR (left) and with 50 μg/L MC-LR (right), respectively. Less SERS nanobioprobes bound with magnetic-bead biosensing substrate because of MC-LR in solution competitively bound with SERS nanobioprobes. c and d, Raman signal intensity decrease with increasing the concentration of MC-LR (0, 0.03, 0.1, 0.3, 1, 3, 10, 20, 50, and 100 μg/L), and the calibration curve of MC-LR detection, respectively. The error bars represent the standard deviations from 8 measurements, which were all within 9.5%.

MC-LR and the average value regarded as effective signal. The SEM image of the MC-LR-coated magnetic bead surfaces after incubation with SERS nanobioprobes showed that many antibody-conjugated nanoparticles bound to a single magnetic bead, providing significant Raman signal amplification. Several nanobioprobes could simultaneously bind to the coated-antigen at one place because the estimated number of hapten molecules attached to the carrier protein (hapten-to-protein molar ratio) BSA determined by MALDI-TOF MS is 6. Fig. 3d shows that, with the higher concentrations of MC-LR, less antibodies bind with the magnetic-beads and, therefore, resultant Raman signals lower. The signal intensities were fitted to a four-parameter logistic

equation (Supporting information). As seen in Fig. 3b, the inverse relationship between Raman signals MC-LR concentration established a dose-response curve for detection of MC-LR over a concentration range from 0.02 to 20 μg/L. A detection limit of 0.01 μg/L for MC-LR was obtained by using $3\sigma/S$ calculation parameter. The sensitivity of this nanobiosensor is further less than the requirements for determination of MC-LR in drinking water as imposed by WHO. The detection limit obtained is also highly comparable to those of SPR detection (0.07 μg/L) (Herranz et al., 2010), electrochemical immunoassay (0.099 μg/L) (Ye et al., 2009), and competitive fluorescence immunoassay (0.03 μg/L) (Yu et al., 2010). The good selectivity of this nanobiosensor was showed by evaluating the nanobioprobe's response to four interfering substances similar to MC-LR (Table S1). Several spiked samples were tested and the recovery of all measured samples was between 80 and 120% with the coefficient of variation less than 10% (Table S2).

3.4. Towards a universal biosensing platform

To demonstrate the general applicability of the design, we also used The Au@DTNB@Ag NRs to label anti-BPA antibody to detect BPA, a xenoestrogenic endocrine-disrupting chemical, which is used in many consumer products worldwide and is widely detected in the environment and in food (Yang et al., 2011). Au@DTNB@Ag NRs was prepared as the Au@PATP@Ag NRs except for DTNB instead of PATP. The sensing mechanism of BPA detection is similar to that of the MC-LR sensing as described above. Fig. 4 shows that the calibration curve for BPA detection was normalized by expressing the signal of each standard point as a ratio to the signal of the blank sample without BPA. The detection limit was estimated to be 0.03 μg/L in the quantification detection range of 0.1–10 μg/L BPA by the definition of the 3σ/slope. These results surpass previous BPA detection studies with amperometric nanobiosensor (Rahman et al., 2007) and graphene-based electrochemical biosensor (Fan et al., 2012), in which sensitivity was ~10 and 1000 times lower, respectively. The BPA detection limits of SERS based nanobiosensor also exceed those of most existing technologies, including standard liquid chromatography (0.3 μg/L) (Szymański et al., 2006) and compact SPR biosensor (0.08 μg/L) (Hegnerová et al., 2010) for BPA detection. Considering the range of Bisphenol A concentrations (< μg/L level) detected in natural waters (Dekant and Voelkel, 2008), the developed nanobiosensor can be used to detect BPA in natural or wastewater samples. From these results, we demonstrated that different SERS nanobioprobes can easily be obtained and applied for the detection of different targets, which proves the versatility of our developed methods. On the other hand, although the SMBP was applied for the detection of single trace analyte in this study, high throughput detection of trace targets can be achieved only in instances where multicolor Raman reporters labeled detection antibodies and magnetic-bead microarray were used.

4. Conclusion

In summary, the development of a universal SERS biosensing platform that can detect a broad range of different molecular targets with high sensitivity and selectivity is highly valuable. Such versatile platforms offer a single solution for tests that have traditionally required the use of a number of different types of instrumentation. Using simple, commercially available magnetic-bead, sandwich structure based SERS nanobioprobes and unsophisticated instrumentation, our technique allows ultralow concentrations of small molecules and protein to be detected in the samples, respectively. The developed nanobiosensing platform demonstrates several advantages: First, the 3-D structure of magnetic-bead provides a perfect platform for binding reaction between capture biomolecules immobilized onto the magnetic-beads and detection antibodies labeled by SERS nanotags, causing reduction of steric effect and assay times and facilitating the separation from homogeneous solution. Second, the sandwich structure of Au@RR@Ag NRs nanotags allows the facile tuning of Raman reporters and high resonance-enhancement, improving the sensitivity of nanobiosensor. Furthermore, one of the advantages of Raman spectroscopy is the narrowband spectrum of the Raman-scattered photons, which leads to the capability for multiplexed detection of analytes. Because we have successfully applied SMBP to achieve the ultrasensitive detection of small molecules and protein, theoretically, high-throughput assays can be achieved through combining the use of magnetic-bead array modified by different captured biomolecules and multicolor SERS tags labeled detection biomolecules. Briefly, our method represents a significant advancement in this domain, as it can provide fundamentally important solutions for rapid screening in drugs

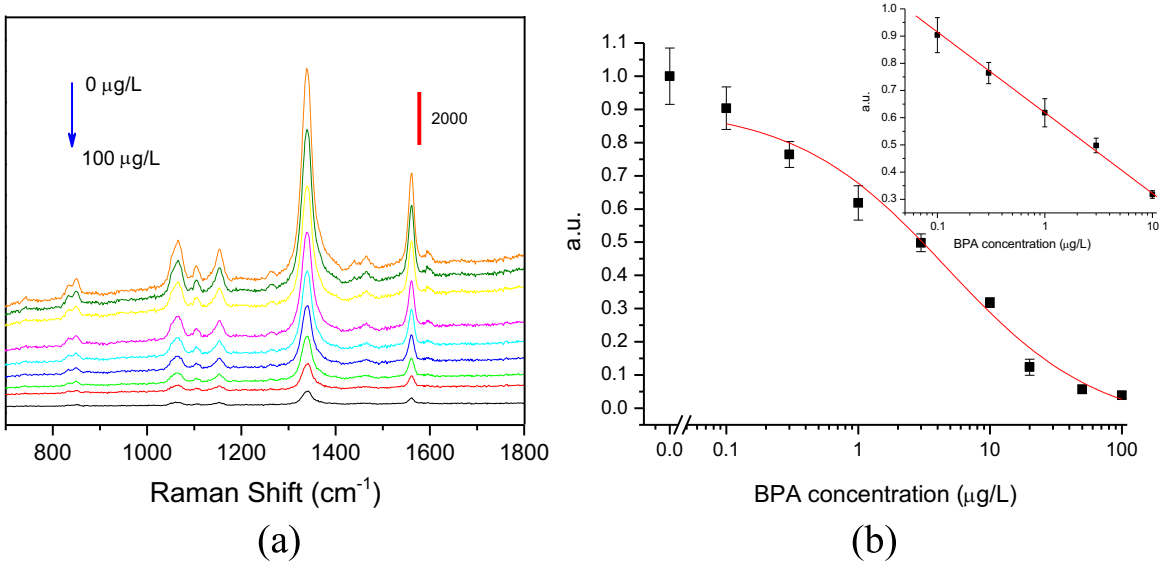

Fig. 4. BPA detection using SMBP. (a) Raman signal decrease with increasing concentration of BPA (0, 0.1, 0.3, 1, 3, 10, 20, 50, and 100 μg/L). (b) The calibration curve of BPA detection usng SMBP. The error bars represent the standard deviations from 8 measurements, which were all within 9.5%.

development, medical diagnosis, point-of-care testing, and environmental monitoring.

Acknowledgments

This research was financially supported by the National Natural Science Foundation of China (21077063, 21277173), the National Instrument Major Project of China (2012YQ3011105), the Special Fund of State Key Joint Laboratory of Environment Simulation and Pollution Control (14K01ESPCT), and the Basic Research Funds in Renmin University of China from the Central Government (13XNLJ01).

Appendix A. Supplementary material

Supplementary data associated with this article can be found in the online version at http://dx.doi.org/10.1016/j.bios.2015.12.108.

References

Anker, J.N., Hall, W.P., Lyandres, O., Shah, N.C., Zhao, J., Van Duyne, R.P., 2008. Nat. Mater. 7, 442–453.
Babak, N., Mostafa, A.E., 2003. Chem. Mater. 15, 1957–1962.
Dekant, W., Voelkel, W., 2008. Toxic. Appl. Pharmac 228, 114–134.
Fan, H., Li, Y., Wu, D., Ma, H., Mao, K., Fan, D., Du, B., Li, H., Wei, Q., 2012. Anal. Chim. Acta 711, 24–28.
Grubisha, D.S., Lipert, R.J., Park, H.Y., Driskell, J., Porter, M.D., 2003. Anal. Chem. 75, 5936–5943.
Hegnerová, K., Piliarik, M., Šteinbachová, M., Flegelová, Z., Černohorská, H., Homola, J., 2010. Anal. Bioanal. Chem. 398, 1963–1966.
Herranz, S., Bocková, M., Marazuela, M.D., Homola, J., Moreno-Bondi, M.C., 2010. Anal. Bioanal. Chem. 398, 2625–2634.
Li, J.F., Huang, Y.F., Ding, Y., Yang, Z.L., Li, S.B., Zhou, X.S., Fan, F.R., Zhang, W., Zhou, Z. Y., Tian, Z.Q., 2010. Nature 464, 392–395.
Li, J.M., Wei, C., Ma, W., An, Q., Guo, J., Hu, J., Wang, C., 2012. J. Mater. Chem. 22, 12100–12106.
Li, M., Cushing, S.K., Jianming, Z., Savan, S., Rebecca, E., 2013. ACS Nano 7, 4967–4976.
Liu, B.H., Yu, F.Y., Huang, X., Chu, F.S., 2000. Toxicon 38, 619–632.
Long, F., He, M., Zhu, A.N., Shi, H.C., 2009. Biosens. Bioelectron. 24, 2346–2351.
Longo, G., Alonso-Sarduy, L., Rio, L.M., Bizzini, A., Trampuz, A., Notz, J., Dietler, G., Kasas, S., 2013. Nat. Nanotech. 8, 522–526.
Marc, V., Kaustabh, K.M., Kevin, D., Young-Tae, C., 2013. Cell 31, 249–257.
Matteo, C., Raphaël, T.H., Cumhur, T., Thomas, L., Martin, A.M.G., 2014. Anal. Chem. 86, 8213–8223.
Murphy, R.M., Slayter, H., Schurtenberger, P., Chamberlin, R.A., Colton, C.K., Yarmush, M.L., 1988. Biophys. J. 54, 45–56.
Ndieyira, J.W., Natascha, K., Logan, S., Cooper, M.A., Abell, C., McKendry1, R.A., Aeppli1, G., 2014. Nat. Nanotech. 9, 225–232.
Nie, S., Emery, S.R., 1997. Science 275, 1102–1106.
Overington, J.P., Al-Lazikani, B., Hopkins, A.L., 2006. Nat. Rev. Drug. Discov. 5, 993–996.
Qian, X.M., Nie, S.M., 2008. Chem. Soc. Rev. 37, 912–920.
Rahman, M.A., Shiddiky, M.J.A., Park, J.S., Shim, Y.B., 2007. Biosens. Bioelectron. 22, 2464–2470.
Stewart, M.E., Anderton, C.R., Thompson, L.B., Maria, J., Gray, S.K., Rogers, J.A., Nuzzo, R.G., 2008. Chem. Rev. 108, 494–521.
Swierczewska, M., Liu, G., Lee, S., Chen, X., 2012. Chem. Soc. Rev. 41, 2641–2655.
Szymański, A., Rykowska, I., Wasiak, W., 2006. Acta Chromatogr. 17, 161–172.
Wang, Y., Yan, B., Chen, L., 2013. Chem. Rev. 113, 1391–1428.
Wu, L., Wang, Z., Zong, S., Huang, Z., Zhang, P., Cui, Y., 2012. Biosens. Bioelectron. 38, 94–99.
WHO, 2004. Guidelines for Drinking Water Quality, 3rd. World Health Organization, Geneva, Switzerland.
Xiang, Y.J., Wu, X., Liu, D., Li, Z., Chu, W., Feng, L., Zhang, K., Zhou, W., Xie, S., 2008. Langmuir 24, 3465–3470.
Yang, C.Z., Yaniger, S.I., Jordan, V.C., Klein, D.J., Bittner, G.D., 2011. Environ. Health Perspect. 119, 989–996.
Ye, W., Liu, X., Tan, J., Li, D., Yang, H., 2009. Harmful Algae 8, 637–644.
Yu, H.W., Kim, L.S., Nguyen, G.H., Kim, I.S., 2010. Aanl. Bioanal. Chem. 398, 2625–2634.
Zhang, R., Dong, Z.C., Jiang, S., Zhang, C., Chen, L.G., Zhang, L., Liao, Y., Aizpurua, J., Luo, Y., Yang, J.L., Hou, J.G., 2013. Nature 498, 82–86.